Journal of Materials Chemistry C

ROYAL SOCIETY OF CHEMISTRY

PAPER

View Article Online
View Journal | View Issue

Cite this: J. Mater. Chem. C, 2026, 14, 9060

Meso-N-linker engineering of benzo[*cd*]indole cyanines for mid-band (850–950 nm) near-infrared absorption and film implementation

Dong Jun Lee,[a] Hyun Kyu Lee,[b] Jun Ho Yoon,[a] Hong Mo Kim,[c] Woo Jin Choi,[a] Suhyeon Kim,[a] Wan Soo Kim,[a] Yoo Sang Kim,[a] Seong Hyun Jang,[a] Tae Gyu Hwang[d] and Jae Pil Kim *[a]

Near-infrared (NIR) absorbing films are essential components of CMOS image sensors, particularly for suppressing unwanted signals in the 750–1100 nm range. However, the mid-band NIR region (850–950 nm) remains challenging to cover due to the limited availability of suitable commercial cyanine dyes, necessitating new molecular design approaches. In this study, five benzo[*cd*]indolenyl heptamethine cyanine dyes were synthesized by introducing a *para*-aniline-based N-linker at the meso position bearing amine (Cy-5npnB), amide (Cy-5npaB), hydrogen (Cy-5npB), ester (Cy-5npeB), and cyano (Cy-5npcnB) substituents. Systematic modulation of the electron-donating and electron-withdrawing strengths of the N-linker enabled λ_{max} tuning over a wide range of approximately 116 nm, which correlated well with trends in LUMO stabilization. UV-Vis-NIR measurements in both solution and COP films confirmed that all synthesized dyes effectively covered the mid-band NIR region, demonstrating that meso-N-linker engineering alone enables precise tuning of the absorption profile within the mid-band NIR region. TD-DFT and RMSD analyses further revealed that the unusually low molar absorptivity of Cy-5npnB originates from its large S_0/S_1 geometric displacement, which reduces Franck–Condon overlap, and that the additional peak near 700 nm corresponds to an S_2 transition involving a HOMO−1 → LUMO excitation. To evaluate applicability in NIR cut-off filters, 3-mixed and 4-mixed films were fabricated. Cy-5npnB exhibited the largest absorbance loss upon film formation due to its strong electron-donating character, whereas Cy-5npaB effectively compensated for the residual 820 nm absorption in the prior 3-mixed system and provided an optimal balance between visible and NIR transmittance (76.8% visible, 2.3% NIR). Moreover, comparison of TGA results with film state thermal behavior revealed that, despite its high T_d in bulk, Cy-5npnB exhibited pronounced thermal degradation in COP films due to extensive S_0/S_1 structural reorganization, highlighting that bulk thermal stability does not necessarily translate to film-state robustness.

Received 27th November 2025,
Accepted 9th February 2026

DOI: 10.1039/d5tc04192a

rsc.li/materials-c

1. Introduction

CMOS (Complementary Metal Oxide Semiconductor) image sensors convert incident light into digital signals and are now widely used in various applications, including digital cameras, smartphones, autonomous vehicles, and security systems.[1] One of the essential components in such systems is the NIR cut-off filter. Because CMOS sensors are based on silicon, whose spectral responsivity differs significantly from that of the human eye, unattenuated NIR light causes reddish color distortion in captured images.[2] Conventional NIR cut-off filters rely on reflective multilayer structures, but these suffer from light leakage and angle-dependent color shifts.[3] In contrast, absorption-type NIR cut-off filters—constructed by incorporating an NIR-absorbing film into the filter structure—can effectively overcome these limitations.

Cyanine dyes, with their strong NIR absorption and high molar absorptivity, are promising candidates for such absorbing layers.[4,5] In particular, dyes absorbing in the mid-band NIR region (850–950 nm) are required to achieve continuous coverage across the full 750–1100 nm near-infrared band. However,

[a] Department of Materials Science and Engineering, Seoul National University, Seoul, 08826, Republic of Korea. E-mail: jaepil@snu.ac.kr
[b] Human Convergence Technology R&D Department, Korea Institute of Industrial Technology (KITECH), Ansan 15588, Korea
[c] Semiconductor Analysis Team, Gyeonggi-do Semiconductor Innovation Center, Advanced Institutes of Convergence Technology, Yeongtong-gu, Suwon-si, Gyeonggi-do 16229, Republic of Korea
[d] Interface Materials and Chemical Engineering Research Center, Korea Research Institute of Chemical Technology (KRICT), Daejeon 34114, Republic of Korea

only a limited number of commercial or reported dyes exhibit strong absorption specifically in this region, underscoring the need for new molecular designs.[6] Prior studies have shown that introducing an N-linker at the meso-position induces a hypsochromic shift in heptamethine cyanines; based on this strategy, we aimed to design benzo[*cd*]indolenyl cyanines with λ_{max} values within 850–950 nm.[7]

In our earlier work, excessive steric hindrance at the N-linker induced pronounced conformational twisting, resulting in reduced molar absorptivity and poor thermal stability in the film state.[8] Accordingly, in this study, we designed N-linker variants with moderate steric demand. Using the aniline-substituted Cy-5npB as the parent dye, we introduced two electron-donating and two electron-withdrawing substituents at the *para*-position of the meso benzene ring, yielding five N-linker–modified dyes. Their optical properties were examined in both solution and COP films, and to address the previously observed absorption gap around 820 nm in a 3-mixed film system, the dyes were integrated into an improved 4-mixed NIR film formulation.[8] Thermal stability was also evaluated through TGA and isothermal heating tests in the film state.

2. Experimental section

2.1. Materials

N,N-Dimethylformamide, sodium acetate, cyclopentanone, 1-iododecane, methylmagnesium iodide, and sodium tetrakis[3,5-bis(trifluoromethyl)phenyl]borate (NaBARF) were purchased from Alfa Aesar. Phosphoryl chloride, aniline, 1,2-dichlorobenzene, acetic anhydride, triethylamine and poly[[octahydro-5-(methoxycarbonyl)-5-methyl-4,7-methano-*1H*-indene-1,3-diyl]-1,2-ethanediyl] were purchased from Sigma-Aldrich. Benzo[*cd*]indol-2(1*H*)-one and 18-crown 6-ether, *N,N*-dimethyl-1,4-phenylenediamine, 4′-aminoacetanilide, aniline, methyl 4-aminobenzoate and 4-aminobenzonitrile were purchased from TCI chemicals. Chloroform, dichloromethane, diethyl ether, ethanol, hydrochloric acid, perchloric acid, and sodium hydroxide were purchased from Samchun Chemicals. Silica gel 60 (0.040–0.063 mm) for column chromatography and analytical TLC plates precoated with silica gel 60 F254 were purchased from Merck. All chemicals and reagents were used as received without further purification. Synthetic details and characterization of compounds are described in the SI.

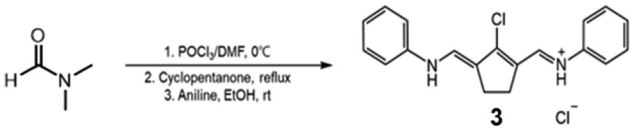

Scheme 2 Synthesis of anilinium salt.

2.2. Structures and synthesis

Benzo[*cd*]indol-2(1*H*)-one was subjected to *N*-alkylation with 1-iododecane to give compound 1. The benzo[*cd*]indolium derivative 2 was then obtained *via* a Grignard addition followed by an acid-mediated elimination using perchloric acid (Scheme 1). The anilinium salts 3 was prepared through a Vilsmeier–Haack process employing *N,N*-dimethylformamide, phosphoryl chloride, cyclopentanone, and aniline (Scheme 2). Subsequently, benzo[*cd*]indolenyl heptamethine cyanine dye Cy-5 was produced by condensing anilinium salts 3 with benzo[*cd*]indolium derivative 2 in the presence of sodium acetate (Scheme 3).

Meso-substitution of Cy-5 was conducted by reacting with *N,N*-dimethyl-1,4-phenylenediamine, 4'-aminoacetanilide, aniline, methyl 4-aminobenzoate and 4-aminobenzonitrile in the presence of triethylamine in DCM/Acetone or DCM or Acetone to yield the Cy-5npn, Cy-5npa, Cy-5np, Cy-5npe, Cy-5npcn respectively (Scheme 4). Finally, the five cyanine dyes were dissolved individually in a dichloromethane/acetone (1 : 1) solvent mixture to introduce bulky counter anions. Ion exchange reactions were then performed by adding NaBARF, forming Cy-5npnB, Cy-5npaB, Cy-5npB, Cy-5npeB and Cy-5npcnB (Scheme 5).

2.3. Fabrication of NIR absorbing films

The cyclic olefin polymer (COP) was employed as the film binder due to its high optical transmittance and thermal durability.[9,10] Poly[[octahydro-5-(methoxycarbonyl)-5-methyl-4,7-methano-*1H*-indene-1,3-diyl]-1,2-ethanediyl], which is a representative COP material, was used as the binder matrix. The COP was dissolved in chloroform to afford a 5 wt% stock solution. Subsequently, the cyanine dyes were added into 1.6 g of this COP stock solution and mixed for 3 min at ambient temperature using a vortex shaker to obtain a homogeneous coating formulation. The prepared coating solutions were then deposited onto pristine glass substrates (50 × 70 × 0.5 mm) by spin-coating.

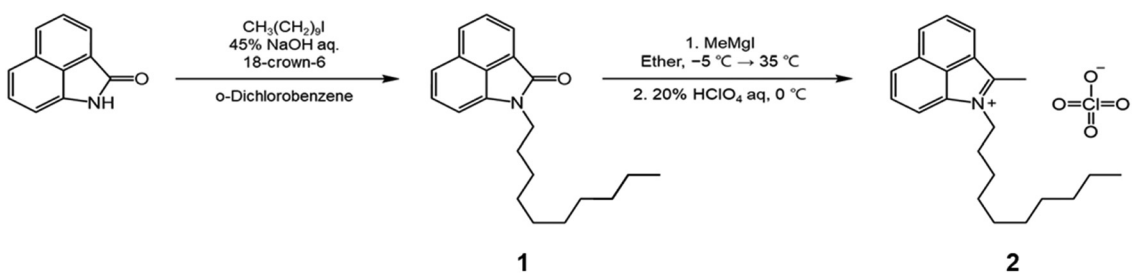

Scheme 1 Synthesis of benzo[*cd*]indolium derivatives **1** and **2**.

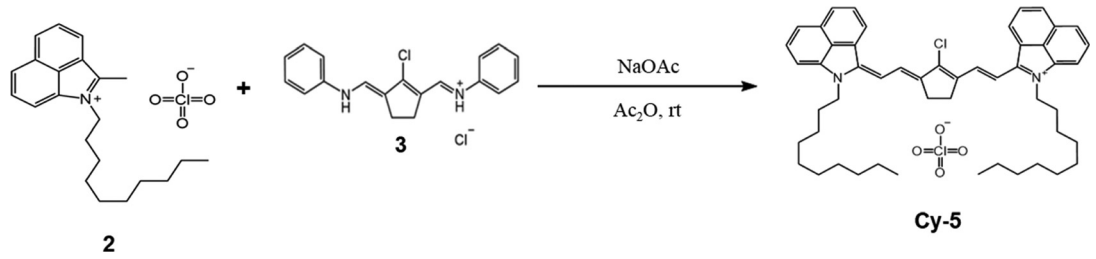

Scheme 3 Synthesis of benzo[*cd*]indolenyl heptamethine cyanine dye (Cy-5).

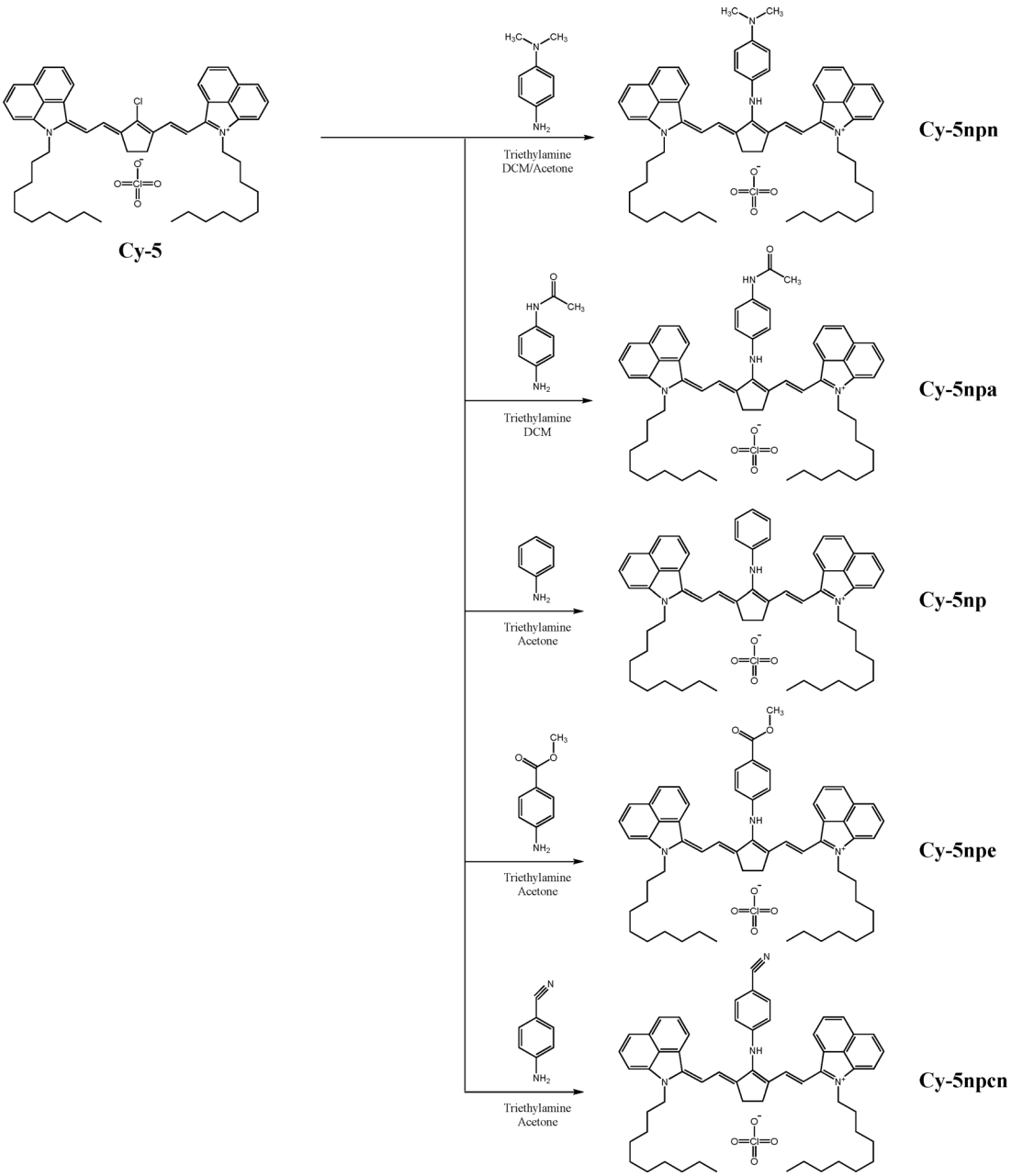

Scheme 4 Synthesis of benzo[*cd*]indolenyl heptamethine cyanine dyes.

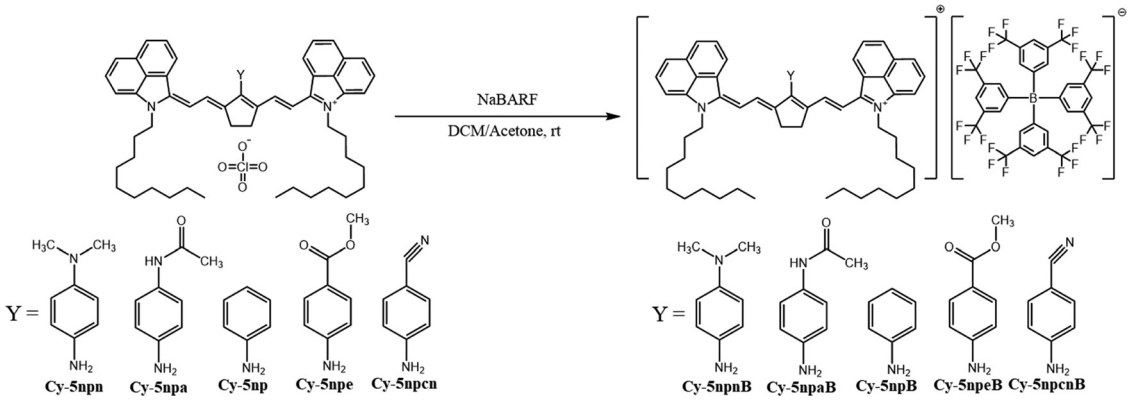

Scheme 5 Substitution of the BARF anion.

2.4. Instruments

1H NMR spectra were recorded on a Bruker Avance III HD spectrometer (850 MHz) using $CDCl_3$ as the solvent. GC/HRMS measurements were performed on a JEOL JMS-700 system. Cold-spray LC-TOF-MS experiments were obtained using a JEOL JMS-T100LP 4G instrument. Thermogravimetric analysis (TGA) was conducted under N_2 using a Mettler Toledo TGA2 with a heating rate of 10 °C min^{-1}. FE-SEM images were acquired using a Carl Zeiss SUPRA 55VP (Pt-coated), and image preparation was carried out using a Leica EM ACE200. UV-Vis-NIR absorption spectra and fluorescence spectra were collected on a Shimadzu UV-1900i and a PerkinElmer LS-55, respectively. Ground-state geometry optimizations were carried out using Gaussian 16 with the B3LYP functional and the 6-31+G(d,p) basis set. Solvent effects were included using the IEFPCM model with dichloromethane. TD-DFT calculations were used to evaluate oscillator strengths of excited states, and additional S_1 geometry optimization was performed to obtain adiabatic transition energies.

3. Results and discussion

3.1. Molecular designs

In designing N-linker-modified cyanine dyes, an aniline unit was selected as the base linker to minimize geometric distortion around the meso-position while preserving effective electronic communication with the polymethine backbone. Electron-donating and electron-withdrawing substituents were systematically introduced at the *para*-position of the aniline ring to enable controlled spectral modulation (Scheme 6).

Specifically, the *para*-substituents were selected to provide a graded electronic series: a strong electron-donating amine group (Cy-5npn), a moderate electron-donating amide group (Cy-5npa), an electronically neutral hydrogen substituent (Cy-5np), a weak electron-withdrawing ester group (Cy-5npe), and a strong electron-withdrawing cyano group (Cy-5npcn). This series was deliberately constructed to span a broad range of electronic effects while maintaining comparable steric environments.

Such an electronically graded design enables systematic modulation of meso-position electronic coupling without altering the core benzo[*cd*]indolenyl polymethine scaffold, thereby

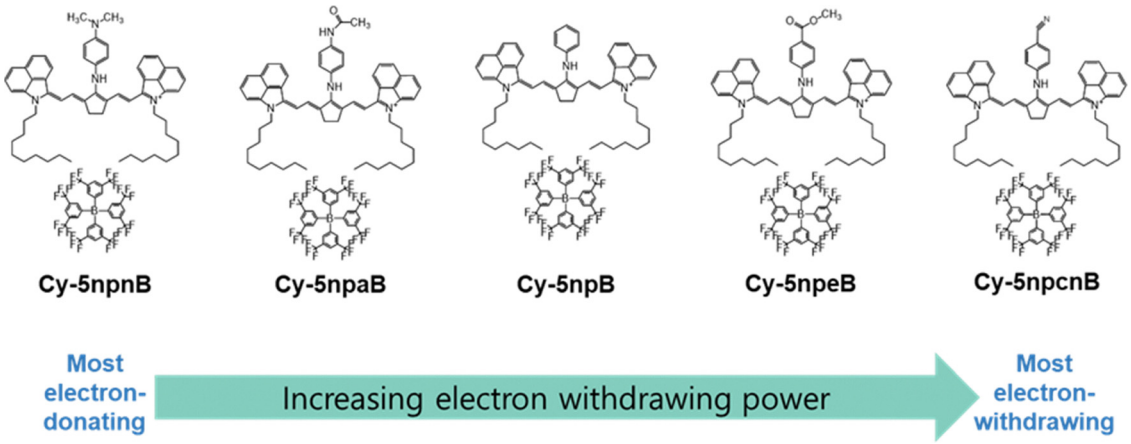

Scheme 6 Introduction of N-linker with electron-donating and withdrawing groups.

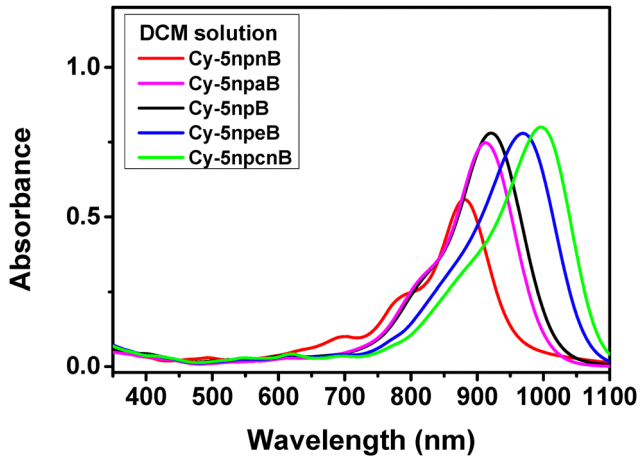

Fig. 1 UV-Vis-NIR absorption spectra of synthesized cyanine dyes in dichloromethane at a concentration of 5×10^{-6}M.

allowing rational investigation of how N-linker electronics influence optical properties.

To further suppress dye aggregation and enhance stability in the film state, the counter cation was exchanged with the weakly coordinating BARF anion $[\{3,5\text{-}(CF_3)_2C_6H_3\}_4B]^-$, affording the final dye series Cy-5npnB, Cy-5npaB, Cy-5npB, Cy-5npeB, and Cy-5npcnB.[11,12]

3.2. Optical characterization

The optical properties of the synthesized cyanine dyes were evaluated using UV-Vis-NIR spectroscopy. The absorption spectra of Cy-5npnB, Cy-5npaB, Cy-5npB, Cy-5npeB, and Cy-5npcnB in dichloromethane are shown in Fig. 1. The corresponding molar extinction coefficients, maximum absorption wavelengths, and full widths at half maximum (FWHM) are summarized in Table 1.

Overall, the synthesized dyes exhibited molar extinction coefficients exceeding 150 000 M^{-1} cm^{-1}, except for Cy-5npnB, which showed a markedly lower value of 112 000 M^{-1} cm^{-1} and a distinctive additional absorption feature around 700 nm. The maximum absorption wavelength progressively red-shifted from Cy-5npnB to Cy-5npcnB, with a total shift of 116 nm, demonstrating that substantial spectral tuning can be achieved solely by varying the electron-donating and electron-withdrawing strength of the *para*-substituted aniline N-linker. In addition, the full width at half maximum (FWHM) increased as the absorption moved to longer wavelengths, indicating broader spectral profiles for the more red-shifted dyes. To elucidate the origins of these optical trends, computational analyses were performed.

3.3. Theoretical calculation

Density functional theory (DFT) is an effective tool for describing both ground and excited state geometries of organic chromophores.[13] Density functional theory (DFT) and time-dependent DFT (TD-DFT) calculations were performed using Gaussian 16. Unless otherwise noted, all calculations were carried out on the isolated cationic dyes without explicit inclusion of the BARF counter anion. The total charge and spin multiplicity were set to +1 and singlet, respectively. Geometry optimizations were performed for the ground state (S_0), followed by TD-DFT calculations on the optimized cationic structures to obtain vertical excitation energies and frontier molecular orbitals. Because BARF is a bulky, weakly coordinating anion, the electronic transitions of the polymethine chromophore are primarily governed by the cationic dye framework. Therefore, calculations on the isolated cation provide a reasonable approximation for discussing intrinsic trends in orbital energies and λ_{max} shifts. The HOMO–LUMO energies and other computed parameters of the N-linker modified dyes, obtained from DFT and TD-DFT calculations, are summarized in Table 2. Although the calculated λ_{max} values deviate from the experimental measurements in absolute magnitude, the overall spectral trends and oscillator strengths show good agreement with the experimental results, confirming the reliability of the computational simulations.

Fig. 2 presents the optimized structures, frontier molecular orbitals, and charge density difference (CDD) maps of Cy-5npn, Cy-5npa, Cy-5np, Cy-5npe, and Cy-5npcn. All N-linker-modified dyes exhibit similar spatial distributions in both the highest occupied molecular orbital (HOMO) and the lowest unoccupied molecular orbital (LUMO), indicating that the S_1 transition primarily involves a local excitation (LE) process.[14,15] In the HOMO, the electron density is distributed toward the terminal hydrogen atoms on the cyclopentene ring for all dyes, whereas in the LUMO, this density disappears and instead becomes localized on the central meso-carbon atom and the attached meso-substituent.

These differences can be more clearly visualized through the charge density difference (CDD) maps, which represent the electron-density redistribution between the HOMO and LUMO. In the CDD plots, the yellow regions indicate an increase in electron density upon excitation, whereas the cyan regions

Table 1 Molar extinction coefficients (ε), the wavelength at maximum absorbance (λ_{max}), and the full width at half maximum ($\omega_{1/2}$) of cyanine dyes in dichloromethane

Dyes	ε (L mol^{-1} cm^{-1})	λ_{max} (nm)	$\omega_{1/2}$ (nm)
Cy-5npnB	112 000	880	101
Cy-5npaB	150 000	913	118
Cy-5npB	156 000	921	125
Cy-5npeB	156 000	969	144
Cy-5npcnB	160 000	996	144

Table 2 LUMO and HOMO enegries (eV), HOMO–LUMO energy gaps ΔE (eV), calculated maximum absorption wavelength λ_{max} (nm), oscillator strength f

Dyes	LUMO (eV)	HOMO (eV)	ΔE (eV)	$\lambda_{max\_calculated}$ (nm)	f
Cy-5npn	−3.537	−5.270	1.733	715.43	2.108
Cy-5npa	−3.630	−5.303	1.672	741.53	2.262
Cy-5np	−3.654	−5.302	1.648	752.33	2.286
Cy-5npe	−3.757	−5.326	1.569	790.21	2.298
Cy-5npcn	−3.805	−5.346	1.541	804.57	2.319

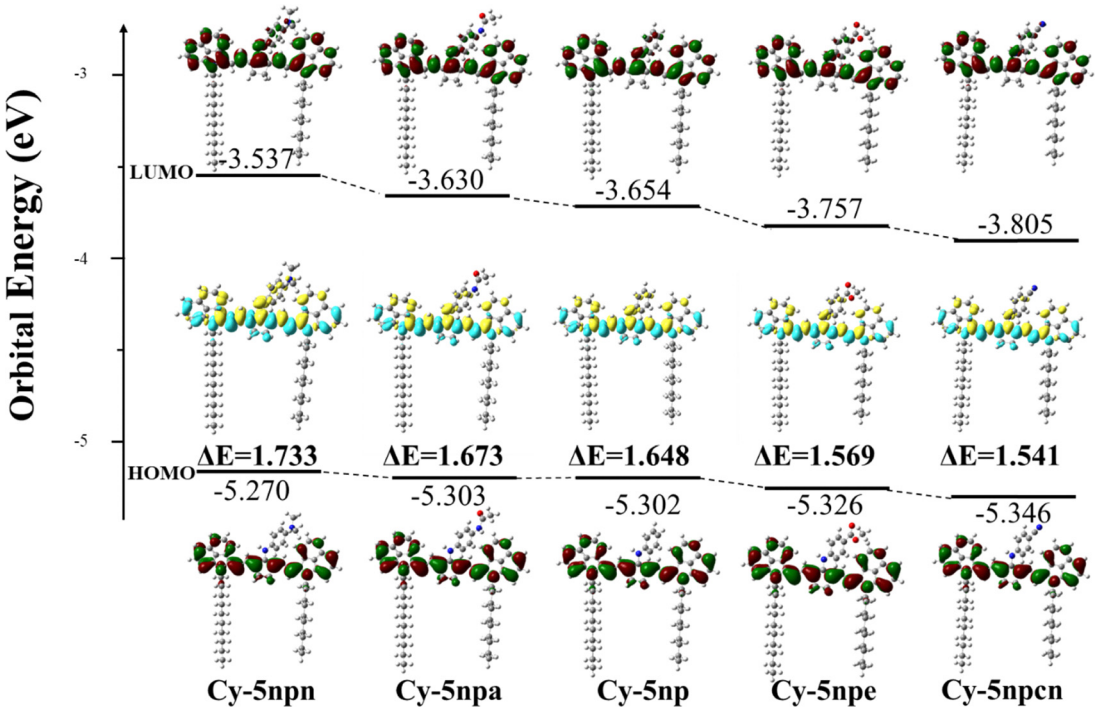

Fig. 2 Frontier molecular orbitals (FMOs) and charge density differences (CDDs) of Cy-5npn, Cy-5npa, Cy-5np, Cy-5npe and Cy-5npcn at the highest occupied molecular orbital (HOMO) and lowest unoccupied molecular orbital (LUMO). The yellow and cyan regions indicate an increase and decrease in the electron density due to excitation, respectively.

represent a decrease. As shown in Table 2, the variation in LUMO energy across the dye series is significantly larger than that of the HOMO. This is because, unlike the HOMO, the LUMO is strongly localized on the meso-position central carbon atom and the attached meso substituent, making it more sensitive to electronic perturbations introduced at this position.

For Cy-5npn, the presence of a strongly electron-donating substituent at the *para*-position of the aniline N-linker destabilizes the LUMO, resulting in the highest LUMO energy level among the series. As the substituent becomes increasingly electron-withdrawing, the LUMO becomes progressively stabilized, ultimately yielding the lowest LUMO energy in Cy-5npcn, which contains the strongest electron-withdrawing group.

As shown in Table 2, Cy-5npn exhibits a noticeably lower oscillator strength than the other dyes, consistent with the experimental observations. To identify the origin of this reduced transition intensity, we compared the optimized geometries of the ground state and the S_1 excited state for each dye, as presented in Fig. 3.

In Fig. 3, the optimized geometries of the ground state and S_1 excited state are shown in black and red, respectively, with both top and side views provided for comparison. In the top views, the meso-position substituents in all dyes except Cy-

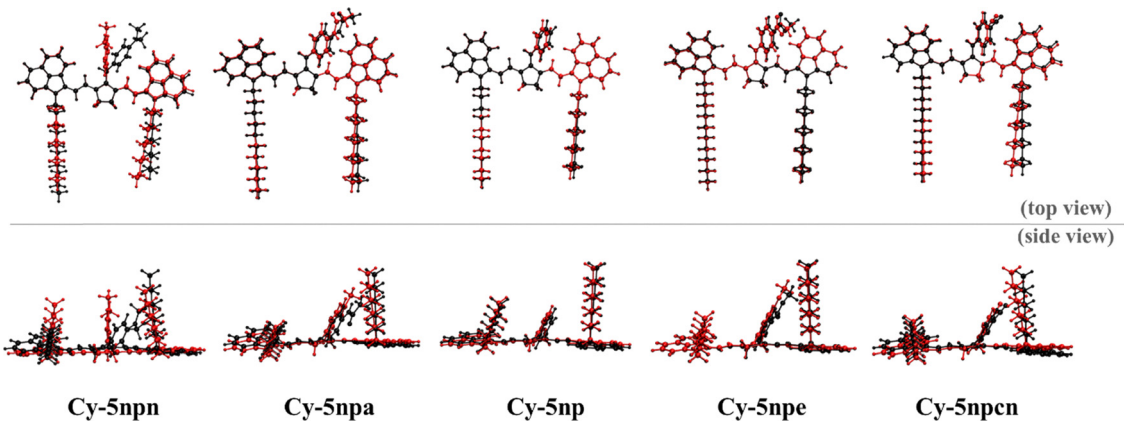

Fig. 3 Superimposed molecular geometries of cyanines comparing the ground state (black) and S_1 excited state (red) conformations optimized at the B3LYP/6-31G+(d,p) level.

Table 3 RMSD values

	Cy-5npn	Cy-5npa	Cy-5np	Cy-5npe	Cy-5npcn
RMSD	1.398	0.293	0.180	0.190	0.118

5npn are bent toward the indole unit on the right side of the molecule, whereas in Cy-5npn, the substituent remains positioned near the center only in the S_1 geometry. The side views further reveal that Cy-5npn exhibits the largest structural deviation between the ground and excited states among the series. To quantify these differences, root-mean-square deviation (RMSD) values between the ground-state and S_1 geometries were calculated using Visual molecular dynamics(VMD), which is a molecular graphics program designed for the display and analysis of molecular assemblies, and the results are summarized in Table 3.[16]

As shown by the RMSD values in Table 3, Cy-5npn exhibits the largest deviation between the ground- and S_1 excited state geometries, consistent with the structural differences observed in Fig. 3. This indicates that Cy-5npn undergoes the most pronounced geometric reorganization upon excitation among the five dyes. Such substantial structural distortion reduces the Franck–Condon overlap, leading to significantly lower molar absorptivity observed for this dye.[8,17]

To further investigate the additional absorption feature around 700 nm observed for Cy-5npnB in Fig. 1, TD-DFT calculations were performed to analyze the S_2 transition. The corresponding frontier molecular orbitals and calculated parameters are summarized in Fig. 4 and Table 4.

Table 4 LUMO and HOMO−1 energies (eV), HOMO−1–LUMO energy gaps ΔE (ev), calculated maximum absorption wavelength λ_{max} (nm), oscillator strength f

Dyes	LUMO (eV)	HOMO−1 (eV)	ΔE (eV)	$\lambda_{max\_calculated}$ (nm)	f
Cy-5npn	−3.537	−5.474	1.937	640.08	0.219
Cy-5npa	−3.630	−5.915	2.285	542.60	0.085
Cy-5np	−3.654	−6.010	2.356	526.25	0.046
Cy-5npe	−3.757	−6.139	2.382	520.50	0.075
Cy-5npcn	−3.805	−6.216	2.411	514.24	0.074

Fig. 4 shows that the S_2 transition corresponds to an electronic excitation from HOMO−1 to the LUMO. The HOMO−1 orbitals are more localized toward the meso-substituent compared to the HOMO orbitals shown in Fig. 2. In particular, Cy-5npn exhibits a strongly localized HOMO−1 density on the aryl substituent at the meso position, with little contribution from the polymethine chain or the indole plane. This pronounced localization raises the HOMO−1 energy level relative to the other dyes. Consequently, as summarized in Table 4, Cy-5npn shows a substantially red-shifted S_2 absorption by nearly 100 nm and a larger oscillator strength. Taken together, these results indicate that the additional peak observed near 700 nm in Fig. 1 for Cy-5npnB originates from this S_2 transition.

3.4. Characterization of NIR absorbing film

The coating solution for the COP films was prepared by mixing 0.004 mmol of each dye with 1.6 g of a 5 wt% polymer solution in chloroform. The resulting formulations were deposited onto

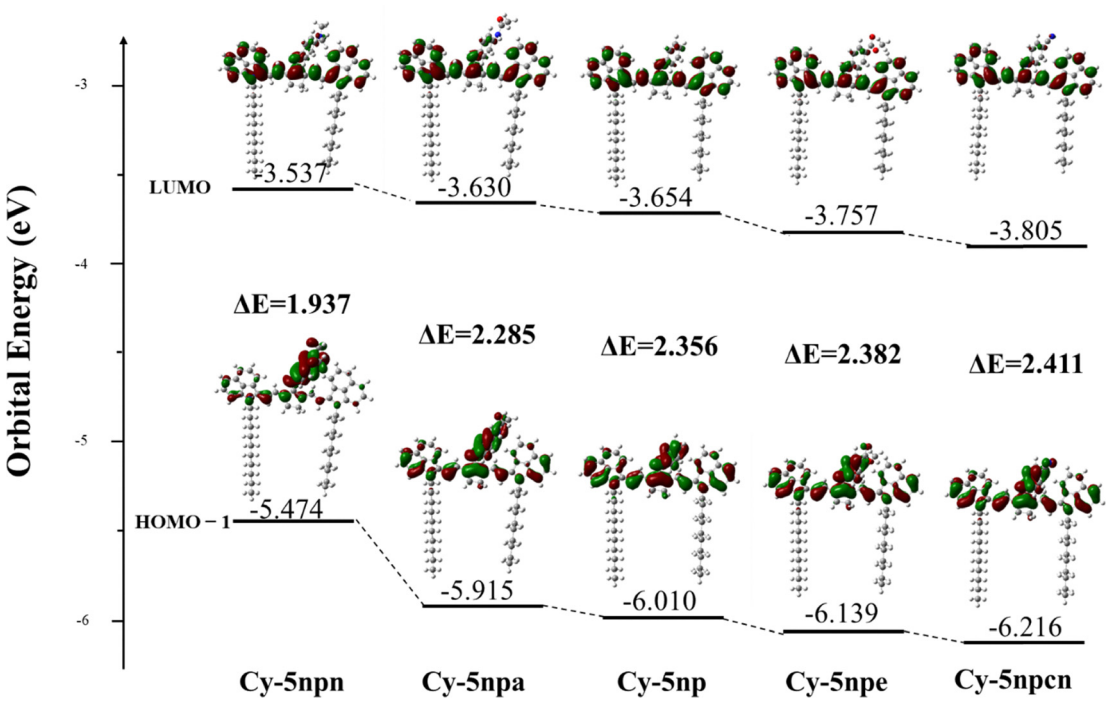

Fig. 4 Frontier molecular orbitals (FMOs) of Cy-5npn, Cy-5npa, Cy-5np, Cy-5npe and Cy-5npcn at the highest occupied molecular orbital −1 (HOMO−1) and lowest unoccupied molecular orbital (LUMO).

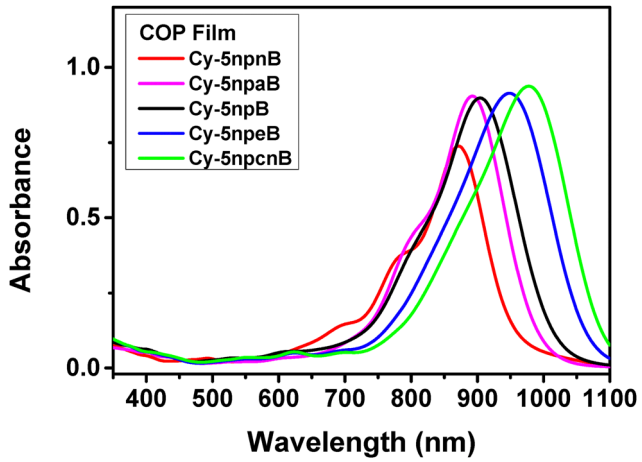

Fig. 5 UV-Vis-NIR absorption of fabricated NIR absorbing films (COP).

Table 5 Absorbance at λ_{max}, the wavelength at maximum absorbance (λ_{max}), and the full width at half maximum ($\omega_{1/2}$) of cyanine dyes in COP films

Dyes	Absorbance at λ_{max}	λ_{max} (nm)	$\omega_{1/2}$ (nm)
Cy-5npnB	0.739	872	143
Cy-5npaB	0.905	892	143
Cy-5npB	0.899	904	153
Cy-5npeB	0.914	949	170
Cy-5npcnB	0.938	978	173

glass substrates by spin-coating at 4000 rpm for 30 s to produce uniform films. The thickness of the COP film was determined by cross-sectional SEM analysis and was found to be 1.504 μm (Fig. S5, SI). The UV-Vis-NIR absorption spectra of the COP films containing Cy-5npnB, Cy-5npaB, Cy-5npB, Cy-5npeB, and Cy-5npcnB, along with their corresponding optical parameters, are presented in Fig. 5 and summarized in Table 5.

In the COP films (Fig. 5), the absorption bands of all dyes appear blue-shifted and broadened compared with those observed in dichloromethane solution (Fig. 1), indicating the formation of H-aggregates in the solid-state environment.[18,19] Consistent with the solution-phase data, Cy-5npnB exhibits both a lower absorbance and a distinctive additional peak near 700 nm in the film state.

We next sought to improve the flatness of the NIR absorption profile in the previously developed 3-mixed film (PhcyB, Cy-5npB, Cy-5pB).[8] To address the remaining absorption gap around 820 nm, additional N-linker dyes were introduced to formulate new 4-mixed films. The absorption and transmittance spectra of the prior 3-mixed system, along with the molecular structures of its constituent dyes, are shown in Fig. 6.

As shown in the transmittance spectrum in Fig. 6(b), the previously developed 3-mixed film exhibits a remaining unattenuated peak near 820 nm. To flatten this region, we introduced additional N-linker dyes with shorter absorption wavelengths than Cy-5npB, specifically Cy-5npnB and Cy-5npaB, to construct new 4-mixed films. The resulting transmittance spectra for each 4-mixed formulation are presented in Fig. 7, and the average visible and NIR transmittance values are summarized in Table 6.

As shown in Fig. 7, the 4-mixed film incorporating Cy-5npnB exhibits lower visible transmittance than the film containing Cy-5npaB. This trend is confirmed quantitatively in Table 6: the Cy-5npnB-based 4-mixed film shows an average visible transmittance of 73.1%, which is approximately 3.7% lower than that of the Cy-5npaB-based counterpart, while its average NIR transmittance is about 0.5% higher. This difference arises

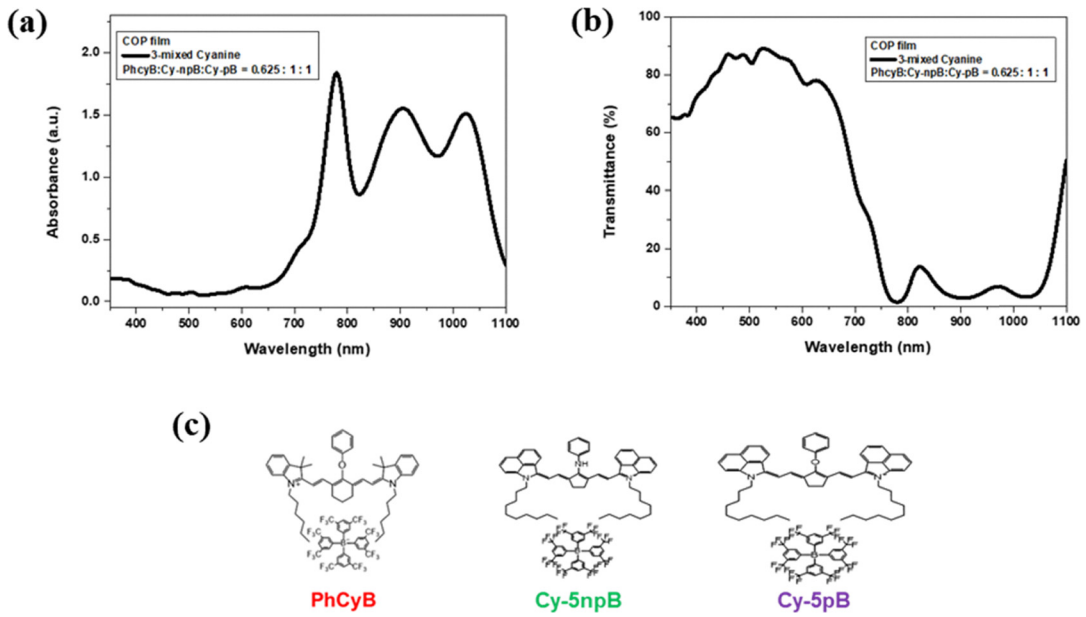

Fig. 6 UV-Vis-NIR absorption (a) and transmittance (b) of fabricated 3-mixed film (COP), molecular structure of cyanine dyes(PhcyB, Cy-5npB, Cy-5pB) in 3-mixed film.

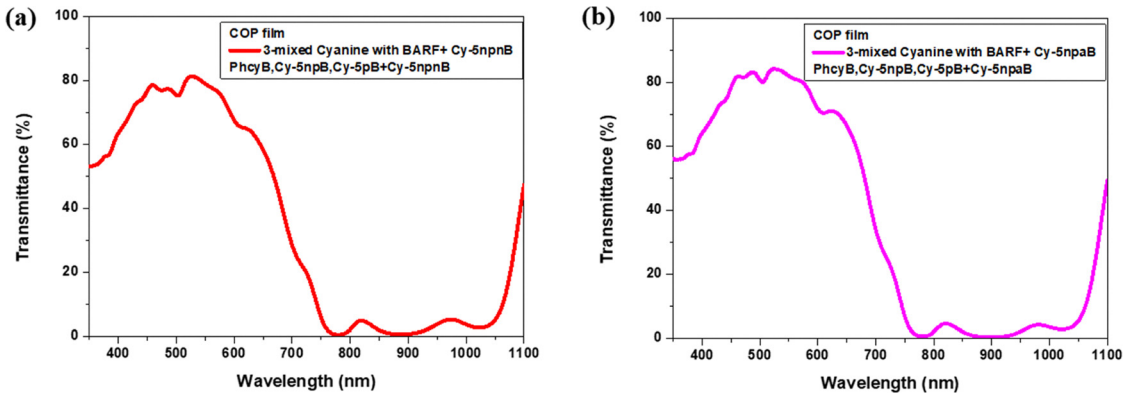

Fig. 7 UV-Vis-NIR transmittance of fabricated 4-mixed films (COP, 3-mixed + Cy-5npnB (a), 3-mixed + Cy-5npaB (b)).

Table 6 Average visible and NIR transmittance of 3-mixed + Cy-5npnB and 3-mixed + Cy-5npaB

Dyes	Average visible transmittance (400–650 nm)	Average near-Infrared transmittance (780–1050 nm)
3-mixed + Cy-5npnB	73.1%	2.8%
3-mixed + Cy-5npaB	76.8%	2.3%

because the lower molar absorptivity of Cy-5npnB requires a higher dye loading to reach the target NIR attenuation, consequently reducing visible transmittance. Based on these results, Cy-5npaB was selected as the optimal fourth component for the 4-mixed film, and its performance is compared with that of the original 3-mixed system in Fig. 8.

For the 3-mixed film shown in Fig. 8, the average visible transmittance was 81.8%, while the average and maximum NIR transmittance were 5.8% and 14.4%, respectively. In comparison, the 4-mixed film exhibited a slightly reduced average visible transmittance of 76.8%, but its average and maximum NIR transmittance decreased significantly to 2.3% and 4.58%. These results demonstrate that the NIR region can be effectively flattened using cyanine dyes alone. Furthermore, the fabrication of the 4-mixed film highlights that, in addition to the maximum absorption wavelength, the molar absorptivity of each dye must be carefully considered when selecting NIR-absorbing components.

3.5. Thermal stability evaluation

In the fabrication of optical filters, dye-containing films are subjected to high-temperature baking processes. Therefore, ensuring sufficient thermal stability of the cyanine dyes is essential for practical and commercial applications.[20,21] To evaluate the thermal robustness of the synthesized dyes, thermogravimetric analysis (TGA) was first performed. The resulting TG curves are shown in Fig. 9 and Fig. 9(b) presents the first-derivative curves, which indicate the temperature ranges in which thermal decomposition begins. Additionally, the temperature corresponding to 2% weight loss was defined as the decomposition temperature (T_d), and the T_d values for each dye are summarized in Table 7.

From the TGA curves in Fig. 9(a), Cy-5npB, Cy-5npeB, and Cy-5npcnB exhibit similar thermal decomposition profiles, whereas Cy-5npnB and Cy-5npaB show noticeably higher thermal stability than the other three dyes. This trend is also evident in the DTG curves in Fig. 9(b), where the onset of decomposition for Cy-5npaB and Cy-5npnB appears at higher temperatures following Cy-5npcnB, Cy-5npB, and Cy-5npeB. Consistent with these observations, the T_d values listed in

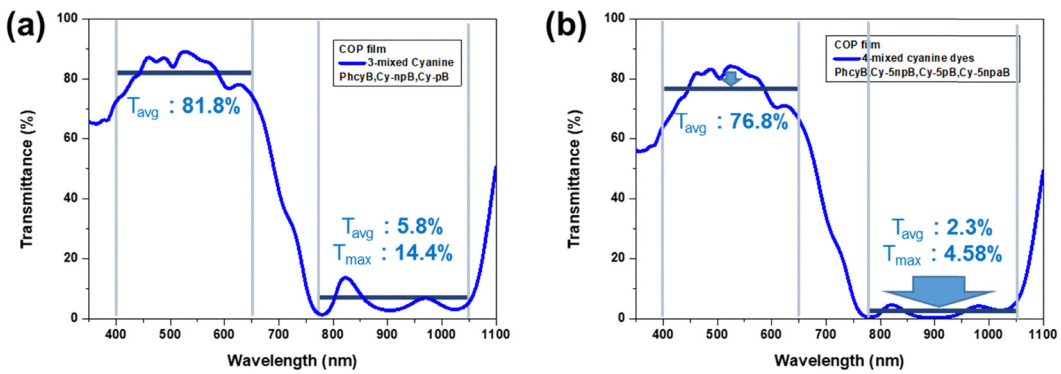

Fig. 8 UV-Vis-NIR transmittance of fabricated 3-mixed(PhcyB, Cy-npB, Cy-pB) film (a) and 4-mixed (PhcyB, Cy-npB, Cy-pB, Cy-5npaB) film.

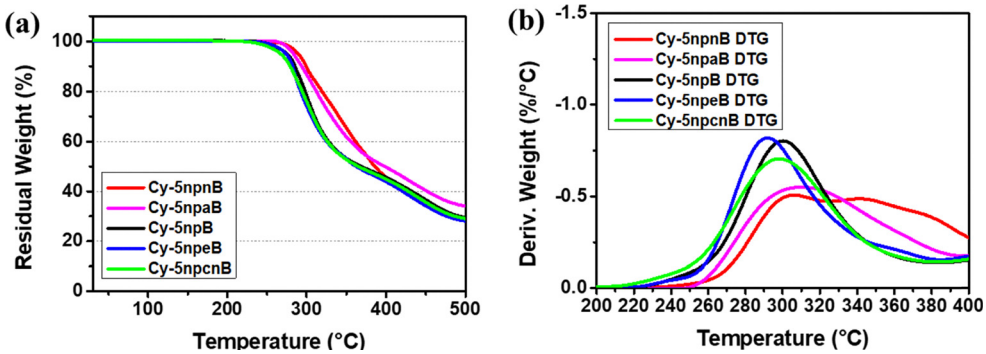

Fig. 9 (a) TGA curves of the synthesized cyanine dyes and (b) first derivative TG curves in the range of initial thermal degradation.

Table 7 Thermal decomposition temperature (T_d) at a 2% weight loss

Dyes	Thermal decompostion temperature (T_d, °C)
Cy-5npnB	278
Cy-5npaB	274
Cy-5npB	260
Cy-5npeB	261
Cy-5npcnB	250

Table 7 indicate that Cy-5npnB possesses the highest decomposition temperature among the series.

The primary origin of these differences can be attributed to the structural changes induced by the introduction of an N-linker in heptamethine cyanines. Incorporation of the N-linker converts the polymethine chain into a bis-dipole configuration, in which the positive charge at the meso-position becomes delocalized when an electron-donating substituent is present, thereby stabilizing the dye and enhancing thermal resistance.[7,8] In contrast, electron-withdrawing substituents localize the meso-positive charge, destabilizing the dye and lowering its thermal stability.

Although Cy-5npeB contains an electron-withdrawing group, its T_d value is comparable to that of Cy-5npB. This behavior can be rationalized by considering that aryl–carbonyl systems often exhibit partial resonance between the ester carbonyl and the aromatic ring, which increases the torsional barrier and favors a more planar and rigid conformation. Such resonance-assisted rigidification can partially offset the destabilizing effect of meso-charge localization, resulting in a T_d similar to that of Cy-5npB.[22–24]

To evaluate the thermal stability of the fabricated COP films, an isothermal heat treatment was carried out. To simulate the TiO_2/SiO_2 thin-film deposition conditions used in CMOS image sensor processing, the COP films were baked at 150 °C for 2 h.[21,25] Prior to baking, all films were subjected to a pre-baking step at 80 °C for 10 min, during which only a slight decrease in absorbance was observed without noticeable changes in spectral shape (Fig. S1, SI).[26] After pre-baking, the films underwent isothermal heat treatment at 150 °C for 2 h, and the resulting absorption spectra are shown in Fig. 10. The relative absorbance changes at the maximum absorption wavelength are summarized in Table 8.

In the magnified absorbance plots in Fig. 10(b), Cy-5npnB exhibits the most pronounced decrease in absorbance. As summarized in Table 8, while the other dyes retained 78.9–85.2% of their initial absorbance after thermal treatment, Cy-5npnB showed a substantial decrease to 47.7%.

Because the glass transition temperature (T_g) of the COP binder (166 °C) is higher than the baking temperature, large-scale polymer relaxation is unlikely to be responsible for the

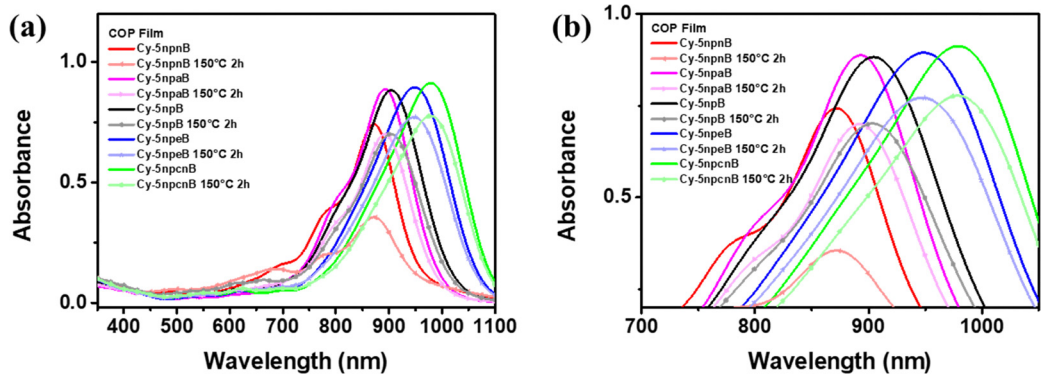

Fig. 10 Change in relative absorbance of NIR-absorbing films before post-baking (solid lines) and after post-baking (symbol lines). (a) Shows the overall absorbance graph, and (b) is an enlarged view around the maximum absorption wavelength.

Table 8 Relative absorbance of NIR absorbing films after the post-baking process

NIR absorbing films	Relative absorbance (A/A_0)	
	Pristine	Baked
Cy-5npnB	1	0.477
Cy-5npaB	1	0.789
Cy-5npB	1	0.795
Cy-5npeB	1	0.863
Cy-5npcnB	1	0.852

observed spectral changes. Although Cy-5npnB exhibits the highest intrinsic decomposition temperature (T_d) in TGA measurements, its poor stability in the film state indicates that bulk thermal decomposition alone cannot explain the spectral changes.

It is also important to note that the TGA measurements were conducted under an inert nitrogen atmosphere, whereas the film baking experiments were performed under ambient air. Thus, the T_d values reflect intrinsic thermal stability in the absence of oxygen, while the film-state stability may additionally involve environmental susceptibility under oxidative conditions. Considering that Cy-5npn possesses the highest HOMO energy among the series, it may be more prone to oxidation during thermal treatment in air. This environmental difference further explains why the film-state stability does not directly correlate with the intrinsic T_d values.

Notably, Cy-5npn contains the strongest electron-donating N-linker among the series. Increased donating strength enhances push–pull interaction along the polymethine backbone and promotes a bis-dipole resonance contribution. The resulting bis-dipole character reduces effective π-electron delocalization and increases bond length alternation (BLA). Indeed, Cy-5npn exhibits the largest BLA value (2.75 pm), whereas Cy-5npcn shows the smallest (1.25 pm) (Fig. S7 and Table S2, SI). The increased BLA reflects enhanced electronic asymmetry and structural polarization along the polymethine chain, which can strengthen intermolecular interactions and promote aggregation in the condensed phase.

Furthermore, Cy-5npn possesses the highest HOMO energy (−5.270 eV), indicating increased electronic destabilization. Consistent with TD-DFT and RMSD analyses, Cy-5npn shows the largest geometric deviation between the S_0 and S_1 optimized structures, indicating pronounced excited-state structural reorganization. In a polymer-embedded environment, such intrinsic electronic asymmetry and structural flexibility can facilitate heat-induced molecular rearrangement or aggregation without requiring chemical bond cleavage.

Therefore, the reduced film-state thermal stability of Cy-5npnB is more plausibly attributed to aggregation-driven structural reorganization and environmental susceptibility rather than simple thermal decomposition. These results highlight that excessive donating strength can induce bis-dipole character, increase BLA, and ultimately compromise film-state stability, underscoring the importance of balancing electronic effects in the molecular design of thermally robust NIR-absorbing cyanine dyes.

4. Conclusion

This work establishes a molecular design framework for precisely tuning mid-band NIR region in benzo[*cd*]indolenyl heptamethine cyanines through systematic modulation of meso-position N-linker electronics. By isolating the electronic effect of the N-linker while maintaining an identical chromophore core, we demonstrate that LUMO stabilization, Franck–Condon overlap, and molar absorptivity can be rationally controlled without altering the fundamental polymethine structure.

Importantly, our results reveal that excessive electron-donating strength induces bis-dipole character, increases bond length alternation (BLA), and amplifies S_0/S_1 geometric distortion, which collectively compromise film-state stability in polymer matrices. This finding highlights that spectral tuning alone is insufficient; excited-state structural behavior and matrix-dependent stability must be simultaneously considered in practical material design.

By integrating electronic structure analysis with thin-film performance evaluation, this study provides actionable design principles for developing thermally robust, absorption-type NIR filters for CMOS image sensors. More broadly, it offers insight into how subtle electronic perturbations in polymethine systems govern both optical transitions and condensed-phase stability, contributing to the rational engineering of functional NIR materials for optoelectronic and imaging applications.

Conflicts of interest

There are no conflicts to declare.

Data availability

The data supporting this article have been included as part of the supplementary information (SI). Supplementary information is available. See DOI: https://doi.org/10.1039/d5tc04192a.

Acknowledgements

Samsung Electronics Co., Ltd supported this work as part of the industry-academia cooperation project. The Institute of Engineering Research at Seoul National University provided research facilities for this work. Special thanks to Y. J. Ko and H. S. Shin of the National Center for Inter-university Research Facilities (NCIRF) for their assistance with NMR and GC/HRMS analyses.

References

1 E. R. Fossum, CMOS image sensors: Electronic camera-on-a-chip, *IEEE Trans. Electron Devices*, 2002, **44**(10), 1689–1698.
2 L. Frey, P. Parrein, J. Raby, C. Pellé, D. Hérault and M. Marty, *et al.*, Color filters including infrared cut-off integrated on CMOS image sensor, *Opt. Express*, 2011, **19**(14), 13073–13080.

3 H. M. Kim, H. K. Lee, S. Kim and J. P. Kim, Near-infrared (NIR) absorbing films based on diimmonium dye and cyanine dye for high-performance NIR cut-off filter, *Dyes Pigm.*, 2022, **207**, 110702.
4 G. Gopika, P. H. Prasad, A. Lekshmi, S. Lekshmypriya, S. Sreesaila and C. Arunima, *et al.*, Chemistry of cyanine dyes-A review, *Mater. Today: Proc.*, 2021, **46**, 3102–3108.
5 J. O. Escobedo, O. Rusin, S. Lim and R. M. Strongin, NIR dyes for bioimaging applications, *Curr. Opin. Chem. Biol.*, 2010, **14**(1), 64–70.
6 C. Shi, J. B. Wu and D. Pan, Review on near-infrared heptamethine cyanine dyes as theranostic agents for tumor imaging, targeting, and photodynamic therapy, *J. Biomed. Opt.*, 2016, **21**(5), 050901.
7 S. Pascal, A. Haefele, C. Monnereau, A. Charaf-Eddin, D. Jacquemin and B. Le Guennic, *et al.*, Expanding the polymethine paradigm: Evidence for the contribution of a bis-dipolar electronic structure, *J. Phys. Chem. A*, 2014, **118**(23), 4038–4047.
8 H. K. Lee, D. J. Lee, H. M. Kim, T. G. Hwang, S. Kim and Y. S. Kim, *et al.*, Collaborative utilization of complementary cyanine dyes for application in broad-range NIR-absorbing films, *Prog. Org. Coat.*, 2025, **208**, 109436.
9 G. Khanarian and H. Celanese, Optical properties of cyclic olefin copolymers, *Opt. Eng.*, 2001, **40**(6), 1024–1029.
10 M. Yamazaki, Industrialization and application development of cyclo-olefin polymer, *J. Mol. Catal. A: Chem.*, 2004, **213**(1), 81–87.
11 H. K. Lee, D. J. Lee, H. M. Kim, T. G. Hwang, Y. S. Kim and S. Kim, *et al.*, Development of benzo [*cd*] indolenyl cyanine dyes for NIR-absorbing films and elucidation of molecular structure–spectroscopic relationship, *J. Mater. Chem. C*, 2024, **12**, 3715–3729.
12 S. W. Woo, J. Y. Kim, T. G. Hwang, J. M. Lee, H. M. Kim and J. Namgoong, *et al.*, Effect of weakly coordinating anions on photo-stability enhancement of basic dyes in organic solvents, *Dyes Pigm.*, 2019, **160**, 765–771.
13 B. Le Guennic and D. Jacquemin, Taking up the cyanine challenge with quantum tools, *Acc. Chem. Res.*, 2015, **48**(3), 530–537.
14 L. K. Reimann, D. D. Fortes, F. D. Santos, H. D. Silva Junior, A. M. Morás, D. J. Moura, R. D. Duarte and F. S. Rodembusch, Near-Infrared-Emitting Meso-Substituted Heptamethine Cyanine Dyes: From the Synthesis and Photophysics to Their Use in Bioimaging, *Chemosensors*, 2023, **11**(1), 47.
15 J. M. Lee, J. M. Park, H. K. Lee, H. M. Kim, J. H. Kim and J. P. Kim, Synergistic effects of photoinduced electron transfer and heavy atom effect based on BODIPY for efficient triplet photosensitizers, *Dyes Pigm.*, 2021, **196**, 109662.
16 W. Humphrey, A. Dalke and K. Schulten, VMD: visual molecular dynamics, *J. Mol. Graphics*, 1996, **14**(1), 33–38.
17 G. Batignani, E. Mai, G. Fumero, S. Mukamel and T. Scopigno, Absolute excited state molecular geometries revealed by resonance Raman signals, *Nat. Commun.*, 2022, **13**(1), 7770.
18 Y. Hirano, Y. Tokuoka, N. Kawashima and Y. Ozaki, Origin of formation of blue-shifted aggregates including H-aggregates in mixed Langmuir–Blodgett films of merocyanine dye investigated by polarized visible and infrared spectroscopy, *Vib. Spectrosc.*, 2007, **43**(1), 86–96.
19 F. Bertocchi, A. Delledonne, G. Vargas-Nadal, F. Terenziani, A. Painelli and C. Sissa, Aggregates of cyanine dyes: when molecular vibrations and electrostatic screening make the difference, *J. Phys. Chem. C*, 2023, **127**(21), 10185–10196.
20 M. Plouzeau, S. Piogé, F. Peilleron, L. Fontaine and S. Pascual, Polymer/dye blends: Preparation and optical performance: A short review, *J. Appl. Polym. Sci.*, 2022, **139**(36), e52861.
21 H. M. Kim, H. J. Lee, H. K. Lee, T. G. Hwang, J. M. Lee and S. Kim, *et al.*, Binder-endowed thermal stability of diimmonium dye-based near-infrared (NIR) absorbing films, *Mater. Chem. Phys.*, 2021, **270**, 124773.
22 S. M. Gutiérrez Sanfeliciano and J. M. Schaus, Rapid assessment of conformational preferences in biaryl and aryl carbonyl fragments, *PLoS One*, 2018, **13**(3), e0192974.
23 K. Szychta, B. Koszarna, M. Banasiewicz, A. Sobolewski, O. O'Mari and J. A. Clark, *et al.*, Conformation of the Ester Group Governs the Photophysics of Highly Polarized Benzo [g] coumarins, *JACS Au*, 2023, **3**(7), 1918–1930.
24 J.-C. Baucom, N. B. Agyemang, T. Trelles, E. Gallicchio and R. P. Murelli, Studies on the configurational stability of Tropolone-Ketone-, Ester-, and Aldehyde-Based chiral axes. The, *J. Org. Chem.*, 2023, **89**(1), 541–552.
25 B. Fan, M. Suzuki and K. Tang, Ion-assisted deposition of TiO 2/SiO 2 multilayers for mass production, *Appl. Opt.*, 2006, **45**(7), 1461–1464.
26 O. Valdes-Aguilera and D. Neckers, Aggregation phenomena in xanthene dyes, *Acc. Chem. Res.*, 1989, **22**(5), 171–177.